Polyhedron 159 (2019) 298–307

Contents lists available at ScienceDirect

Polyhedron

journal homepage: www.elsevier.com/locate/poly

A mixed valence Tb(III)/Tb(IV) metal–organic framework: Crystal structure, luminescence property and selective detection of naproxen

Chao-Yang Wang [a], Baoyi Yu [b], Huifen Fu [a], Peng Wang [a], Chong-Chen Wang [a,*]

[a] Beijing Key Laboratory of Functional Materials for Building Structure and Environment Remediation, Beijing University of Civil Engineering and Architecture, Beijing 100044, China
[b] Key Laboratory of Urban Agriculture (North China), Ministry of Agriculture, College of Biological Sciences Engineering, Beijing University of Agriculture, Beijing 102206, China

ARTICLE INFO

Article history:
Received 20 October 2018
Accepted 30 November 2018
Available online 15 December 2018

Keywords:
Metal–organic framework
Mixed valence
Luminescence sensor
Selective detection
Naproxen

ABSTRACT

A mixed valence terbium metal–organic framework (MOF), $[Tb_2(HCOO)(clhex)\cdot 2H_2O)]\cdot 2H_2O$ (**BUC-68**) was obtained from the reaction of 1,2,3,4,5,6-cyclohexanehexacarboxylic acid (H_6clhex), formic acid, N, N-dimethylformamide (DMF) and the terbium salt under hydrothermal condition at 140 °C. The crystallographic analysis revealed that the three-dimensional **BUC-68** is composed of two-dimensional $[Tb_2(clhex)\cdot 2H_2O)]$ sheets linked by formic ligand. X-ray photoelectron spectra (XPS) analysis revealed that there were terbium (III) and terbium (IV) presented in **BUC-68**. Thermogravimetric analysis (TGA) indicated that **BUC-68** was stable up to 350 °C. Photoluminescent measurement showed that **BUC-68** displays strong luminescence emission, which was arose from efficient ligand to metal energy transfer transitions. Finally, **BUC-68** was utilized to conduct selective detect of naproxen (NPX) and some small organic molecules.

1. Introduction

Metal–organic frameworks (MOFs), as a new class of hybrid porous materials, arose increasing interests from researchers resulting from not only their diverse structures, tunable pore size and topological diversities [1–5], but also their potential applications like adsorption/separation [6–14], photocatalysis [15–20], gas storage [21–24], drug delivery [25,26], and fluorescent sensor [27–30]. Recently, mixed valence MOFs constructed from Cu(I)/Cu(II) [31], Fe(II)/Fe(III)[32–34], Mn(II)/Mn(III) [35] and Ti(III)/Ti(IV) [36] as templates arose wide interests, due to their unique properties like electrochemical activity [37], magnetism [38], photochromic [39], Néel N-type ferrimagnetism and proton conduction [40]. Up to now, just three mixed valence lanthanide MOFs have been in situ synthesized, i.e. $\{(bpy)_{0.5}(Dy_3(ip)_4(phen)_4(H_2O)\}\cdot 2H_2O\}_n$ [41], $^3_\infty[Eu_3(Tz^*)_6(Tz^*H)_2]$ [42] and $Sr(HCOO)_2$: Eu^{2+}/Eu^{3+} [43]. Lanthanide metal–organic framework are produced lanthanide based metal–organic frameworks are of interest resulting from their narrow emission and high color purity resulting from the Ln(III) irons [44], and their luminescent intensities can be enhanced by the f-f transitions via an "antenna effect" [45]. Ln-based emissions are sensitive to the chemical environment, which makes them be widely used as fluorescent probes for pollutants sensing like poisonous gases, organic solvents, and heavy metals [46–48]. The mechanisms of the luminescence are mainly assigned to metal-centered (MC), ligand-centered (LC) and charge transfer (CT) emissions, respectively. Recently, some Ln-MOFs were even used as selective probe and efficiently separate cationic or anionic dye molecules from their matrix due to the host–guest electronic interactions, guest–guest exchange interactions, Förster resonance energy transfer (FRET), radiative energy transfer and Dexter electron exchange (DEE) [49,50].

The syntheses of lanthanide MOFs (Ln-MOFs) are challenging tasks considering the large radii and high coordination number of lanthanide metals, and lanthanide ions have a high affinity to oxygen atoms [51,52]. The polydentate 1,2,3,4,5,6-cyclohexanehexacarboxylic acid (H_6clhex) was used to build some Ln-MOFs architectures [53–56]. The partly or completely deprotonated H_n-$clhex^{n-6}$ exhibited various coordination modes like monodentate, bridging and chelating [53,57] (as shown in Scheme S2) resulting from its different conformations like **I** (a,e,a,e,a,e), **II** (e,e,e,e,e,e), **III** (e,e,e,e,a,a), **IV** (e,e,e,e,a,e), **V** (e,e,a,e,e,a) and **VI** (e,e,e,e,e,a), respectively (a is axial conformation and e is equatorial conformation) [57]. According to the previous literatures [58], the multifunctional $H_n clhex^{n-6}$ ligand is effective to collect and transfer light to metal ions in the corresponding MOFs to generate fantastic luminescence [49]. With this paper, a novel Tb(III)/Tb(IV) mixed valence MOF $[Tb_2(HCOO)(clhex)\cdot 2H_2O)]\cdot 2H_2O$ (**BUC-68**) was presented, in which its crystal structure, thermal stability, luminescent property along with their sensing application were

* Corresponding author. Fax: +86 10 61209186.
E-mail address: wangchongchen@bucea.edu.cn (C.-C. Wang).

https://doi.org/10.1016/j.poly.2018.11.064
0277-5387/

investigated. **BUC-68** can emit characteristic luminescence resulted from Tb(III) ions and the "antenna effect" from H_6clhex ligand [45,59]. As well, **BUC-68** was utilized to act as probe to selectively detect PPCPs (Pharmaceutical and Personal Care Products) and some small organic molecules.

2. Experimental section

2.1. Materials and instruments

All chemicals were commercially available and used directly as received without any further treatment. Elemental analyses of C, H and N of the MOFs were obtained using an Elementar Vario EL-III instrument. The crystal structures of the prepared powders were performed on a Dandonghaoyuan DX-2700B diffractometer using Cu Kα radiation with 2θ ranging between 5° and 50° at a scanning rate of 0.5°·min^{-1}. Infrared (IR) spectrum was recorded on a Nicolet-6700 Fourier transform infrared spectrophotometer in the region (400–4000 cm^{-1}). Thermogravimetric analyses were performed from 70 to 800 °C in an air stream at a heating rate of 10 °C ·min^{-1} on a DTU-3c thermal analyzer with α-Al_2O_3 as a reference. UV–Vis diffuse reflectance spectrum (DRS) of solid sample was measured from 200 to 800 nm with a PerkinElmer Lamda 650S spectrophotometer, in which $BaSO_4$ was used as the standard with 100% reflectance. Luminescence spectra were recorded on a Hitachi F-7000 spectrophotometer at room temperature. The lifetime was recorded on an Edinburgh FS5 spectrophotometer at room temperature.

2.2. Synthesis of BUC-68

A mixture of H_6clhex (0.3 mmol, 0.1045 g), $TbCl_3{\cdot}6H_2O$ (0.3 mmol, 0.1120 g), deionized water (7 ml) and DMF (7 ml), with a molar ratio of 1:1:1296:1296, was sealed in a 25 mL Teflon-lined stainless steel Parr bomb, heated at 140 °C for 72 h under autogenous pressure and then cooled down to room temperature. White block crystals were isolated and washed with deionized water and ethanol (yield: 86% based on $TbCl_3{\cdot}6H_2O$). *Anal.* Calc. for **BUC-68**, $C_{13}H_{15}O_{18}Tb_2$, C, 20.09; H, 1.95; O, 37.06. Found: C, 20.12; H, 1.98; O, 37.11%. IR(KBr)/cm^{-1}: 3424, 1591, 1422, 1306, 1269, 1201, 1066, 1038, 1021, 935, 824, 813, 710, 604, 518, 460.

2.3. X-ray crystallography

X-ray single-crystal data collection for **BUC-68** was recorded with a Bruker CCD area detector diffractometer with graphite-monochromatized MoKα radiation (λ = 0.71073 Å) using the ψ-ω mode at 293(2) K. The Smart software [60] and SAINT software [61] were used for X-ray single-crystal data collection and data extraction respectively. Empirical absorption corrections were performed with the Sadabs program [62]. The structures were solved by direct methods (Shelxs-2015) [63] and refined by full-matrix-least squares techniques on F^2 with anisotropic thermal parameters for all of the non-hydrogen atoms (Shelxl-2015) [63]. All hydrogen atoms were located by Fourier difference synthesis and geometrical analysis. These hydrogen atoms were allowed to ride on their respective parent atoms. All structural calculations were carried out using the Shelx-2015 program package [63]. The crystallographic data and structural refinements for **BUC-68** are summarized in Table S1. Selected bond lengths and angles are listed in Table S2.

2.4. Luminescence performances test

The luminescence experiments were carried out at ambient conditions in a 5 ml tubes containing 4 mg of **BUC-68** and 4 mL of target solution. The suspension was dispersed well by shaking, and then determined after equilibrium for 5 min.

3. Results and discussion

3.1. Characterizations

BUC-68 is stable under air and in common solvents like ethanol, methanol, acetone, and N,N-dimethyl formamide (DMF), and the corresponding PXRD patterns were shown in Fig. S1. The FTIR spectrum of **BUC-68** was illustrated in Fig. S2. The strong absorption at 3424 cm^{-1} is assigned to stretching vibration of hydroxyl, implying the presence of water molecules [64,65]. The characteristic bands at 1591 cm^{-1} and at 1422 cm^{-1} are assigned to asymmetric stretching (ν_{as}) and symmetric stretching (ν_s) of carboxylic groups, respectively [66]. The value of the difference ($\Delta\nu$) between ν_{as} and ν_s is about 197 cm^{-1}, indicating that the oxygen atoms of carboxylate group were coordinated to Tb via bidentate mode [67].

3.2. Crystal structure description

The completely deprotonated clhex^{6-} anion adopted e,e,e,e,e,e-conformation (as illustrated in Fig. 1, t), in which the central ring displayed chair-shaped configuration and the carboxylate groups located at the equatorial positions, comparable to that observed in the previous studies like $[Tb_4(L_{II})(ox)_3(H_2O)_8]$[68]. All the oxygen atoms from the carboxylate groups attached to clhex^{6-} anions were engaged in coordination to the Tb ions via chelating mode like $\eta^{12}\mu_6$ one as illustrated in Scheme 1(I). Generally, H_6clhex can display various coordination modes as illustrated in Scheme 1. For example, Wang et al. reported three-dimensional lanthanide MOF $[Tb_4(L^{II})(ox)_3(H_2O)_8]$ [68], in which the ligand H_6lhex exhibits the coordination mode of II. Tong *et al.* synthesized two MOFs $[Cd_{12}(\mu_6\text{-}L^{II})(\mu_{10}\text{-}L^{II})_3(\mu_2\text{-}H_2O)_6(H_2O)_6]{\cdot}16.5H_2O$ and $Na_{12}[Cd_6(\mu_6\text{-}L^{II})(\mu_6\text{-}L^{III})_3]{\cdot}27H_2O$, in which the mode (III) and (IV) of H_6lhex were adopted for the former one, while the coordination mode (III) and (V) were presented in the later one (Scheme 1) [69]. Different conformation modes of H_6clhex also have different structural stability. Previous studies have demonstrated the stability of different conformations, which are $L^{V} > L^{II} > L^{III} > L^{VI} > L^{IV} > L^{I}$ (H_6lhex) respectively [57,70]. According to the literatures [57,71,72], the conformations of H_6clhex (L) was speculated that the approach of metal ions to L can activate and remove the α-protons on the ligand, leading to a metastable state L^* was formation at the same time, the carboxylate groups rapidly adopt their optimal positions and coordinate to the ions. Inspired by the previous reports, Tb ions may adopt this reaction process in this study. A further speculation can be acquired that mixed valence (III/IV) lanthanide metal ions can also exist this conformational transformation (Scheme 2).

In **BUC-68**, each Tb atom is nine-coordinated by six oxygen atoms from three clhex^{6-} anions, one oxygen atoms from a formic acid ligand and two oxygen atoms from two different aqua ligands to complete a slightly distorted tricapped trigonal prism. The Tb–O distances were comparable to the normal values for these bonds as found in counterpart MOFs (Table S2) [75,76].

In **BUC-68**, cationic Tb centers are coordinated by the $\eta^{12}\mu_6$ clhex^{6-} anions to construct a 2D metal–organic layers viewed along *ab* plane, as demonstrated in Fig. 1c. The layers are stacked along the *b* axis following the ABAB sequence, in which the Tb ions of the odd layers were located above the triangular hollows of the

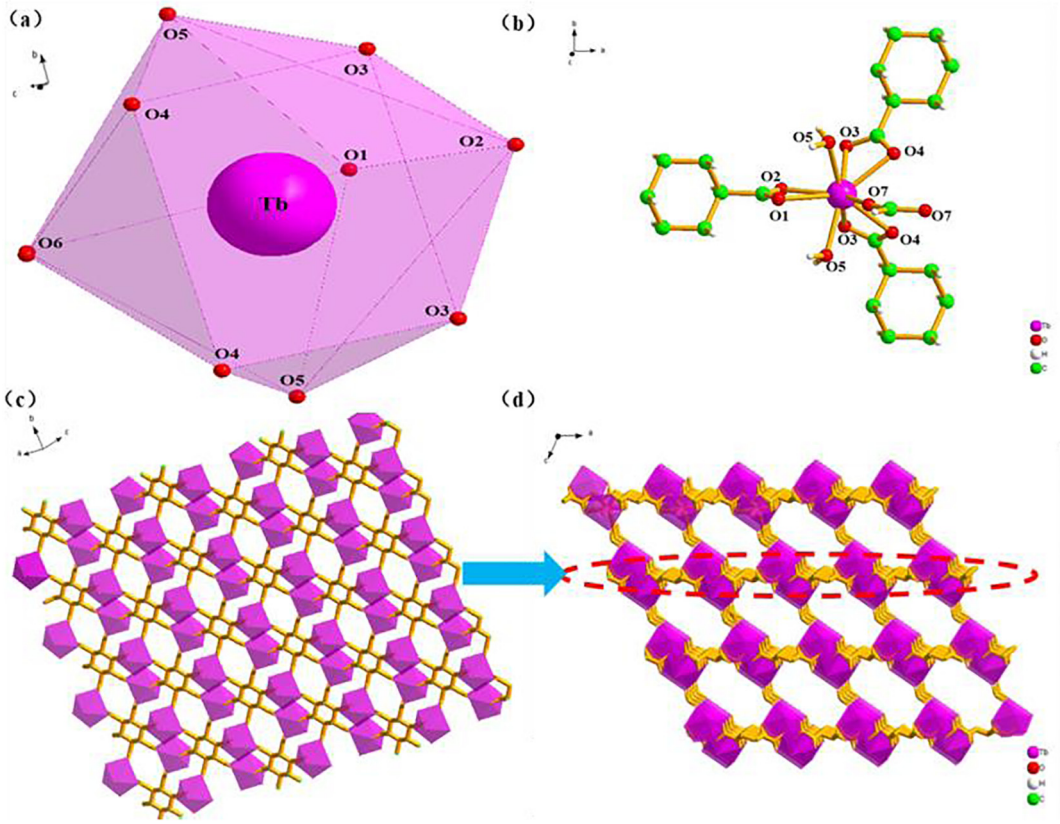

Fig. 1. (a) Highlight of the coordination polyhedron for the Tb atom; (b) The secondary building unit of TbO9; (c) The 2D sheet of **BUC-68**; (d) the 3D structure of **BUC-68**.

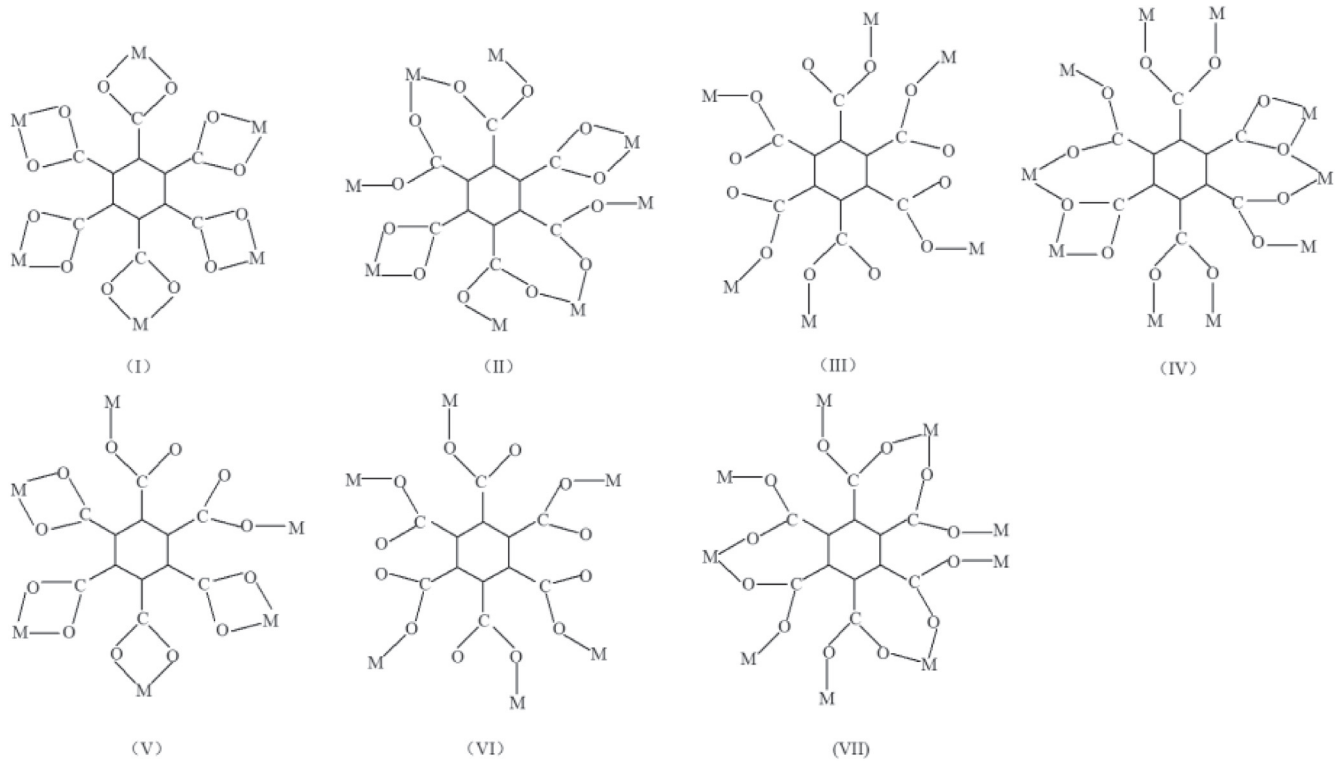

Scheme 1. Coordination mode of H_6Ihex in Compound (I, II [69,73], III~VI [69], VII [74]) [53].

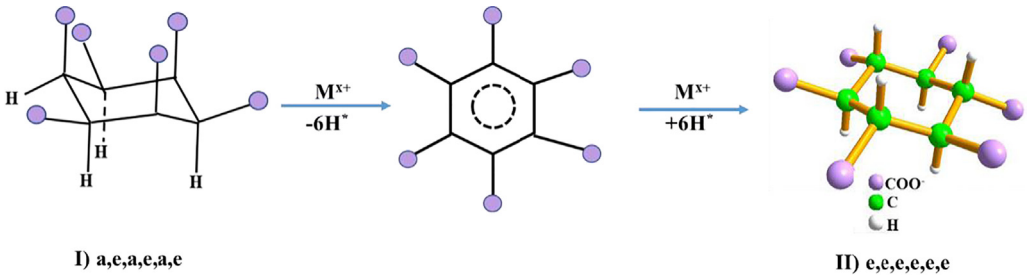

Scheme 2. Possible reaction mechanism of the conformational conversion of the H_6clhex ligand [74].

even ones, which blocked the formation of channels [56]. As shown in Fig. 1, the thickness of the layer is about 0.6646 nm viewed along the *b* axis. Just one type of distorted quadrangular pores with dimensions 0.9889 nm × 0.6653 nm can be found in the layers along the *b* axis (Fig. 1c). Meanwhile, the formate ligands adopting the bidentate bridging mode (Scheme S1, e) connect the Tb1 atoms to form a one-dimensional chain. The one-dimensional chain linked the neighboring Tb1 atoms along *b* axis to form the main chain in the structure of **BUC-68**. The neighboring layers were joined by the one-dimensional chain via Tb-O interaction of three H_6clhex carboxylate groups to produce the final three-dimensional structure of **BUC-68** (Fig. 1(d)). It was worthy to noting that the C5, H5, O6 and O7 in the deprotonated formate ($HCOO^-$) are disordered over two sites with occupancy factor ratio of 0.5/0.5. In the three-dimensional structure of **BUC-68**, the distorted quadrangular channels in the framework were occupied by the two coordinated aqua ligands to further stabilize the crystal structure.

It was interesting to find that two different valance state Tb, i.e. Tb(III) and Tb(IV), were presented in the **BUC-68**. To understand the above speculation, the X-ray photoelectron spectra (XPS) of **BUC-68** has been determined. As shown in Fig. 2, the peaks at 1240.14 and 1276.53 eV are assigned to $3d_{5/2}$ and $3d_{3/2}$, which are characteristic peaks of Tb(III); while the peaks at 1243.14 and 1250.81 eV are assigned to the $3d_{5/2}$ of Tb(IV) [77,78]. It's known that the redox trend of lanthanide ions depends on the 4f → 5d transition energy and the charge-transfer energy from the host anion to the lanthanide ions [79]. Tb(III) is characterized by very low 4f → 5d transition energies and very high charge-transfer energies [80]. The electron configuration of terbium is $[Xe]4f^96s^2$, which made it easy for Tb(III) to lose an electron and be oxidized into Tb(IV) [81]. Blasse et al. reported that Tb(III) is unstable and tends to oxidize into Tb(IV), especially in cubic phase materials [82]. The presence of Tb(IV) in **BUC-68** can be further affirmed by the off-white solids on its Fluorescence surface upon the excitation of 254 nm (Fig. 2 inset) [83–85].

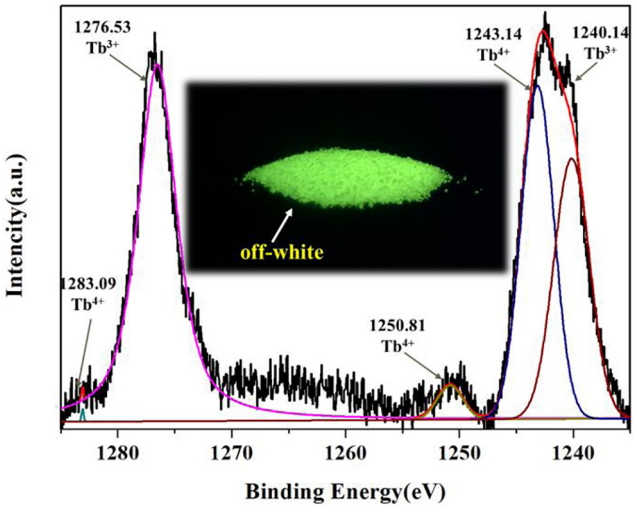

Fig. 2. XPS deconvoluted scans and fittings results for the selected peaks of Tb(III) and Tb(IV) in **BUC-68** (inset: photochromic effects of **BUC-68** under excitation at 254 nm light).

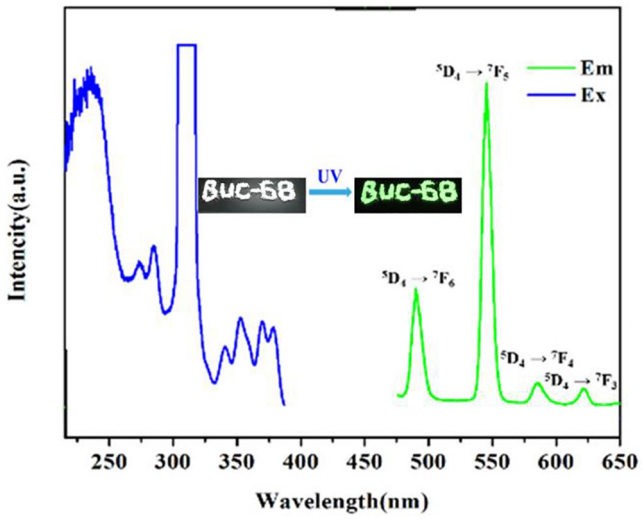

Fig. 3. Luminescence spectra of **BUC-68** in solid state at room temperature (excited and monitored at 230 nm and 545 nm, respectively).

3.3. Fluorescence properties

The fluorescence property of **BUC-68** was investigated in the solid state at room temperature, which revealed that **BUC-68** showed distinct luminescence in the visible range under UV-light excitation. As illustrated in Fig. 3, it can be observed that **BUC-68** possesses wide luminescence band centered at 489, 545, 589 and 621 nm, corresponding to $^5D_4$–$^7F_6$, $^5D_4$–$^7F_5$, $^5D_4$–$^7F_4$ and $^5D_4$–$^7F_3$ f-f transitions of Tb(III) ions, respectively [86]. As illustrated in Fig. S3, the decay lifetime of **BUC-68** is 0.82 ms, comparable to the reported MOFs [87,88]. The long lifetimes may be attributed to the strong chelating coordination and the stable structure of $clhex^{6-}$, which provide an effective pathway for energy transfer [89].

As is shown in Fig. S4, the luminescence intensity of **BUC-68** at 545 nm is 28 times higher than that of terbium hexahydrate chloride (solid state), which can be attributed to "antenna effect" [48,90,91] resulted from the efficient energy-transfer between ligand and Tb(III). UV–Vis absorption spectra of **BUC-68** and H_6-clhex were illustrated in Fig. 4(b), in which the absorption spectra of **BUC-68** matches well with the UV–Vis spectra of H_6clhex,

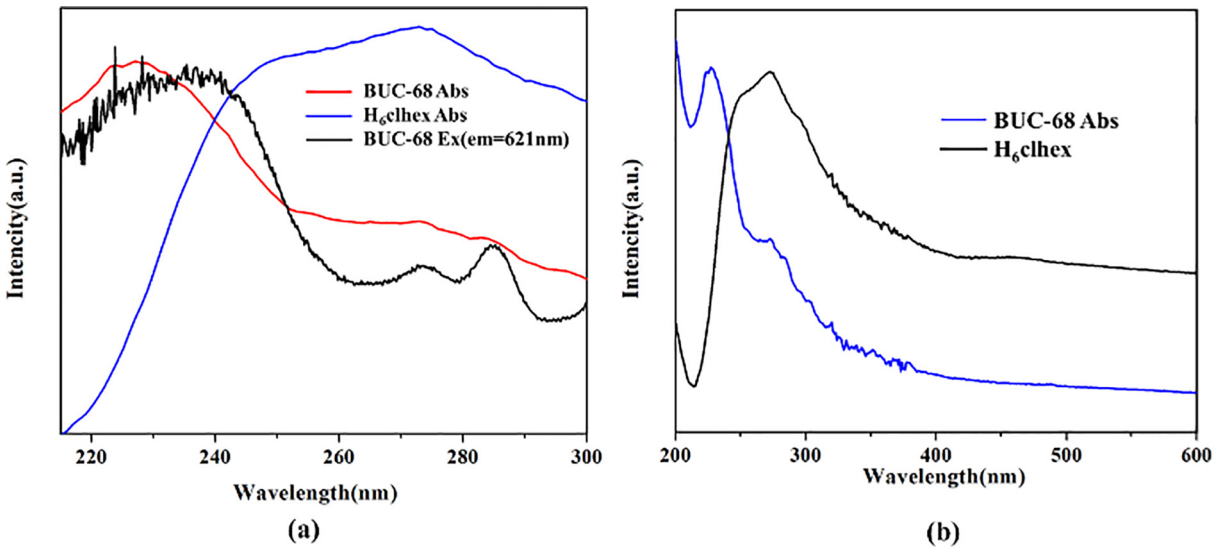

Fig. 4. (a) Absorption and excitation spectra of **BUC-68** in solid state, and the absorption spectra of H_6clhex at room temperature (220∼300 nm); (b) UV–Vis spectra of **BUC-68** and H_6clhex in solid state at room temperature (200∼600 nm).

implying that H_6clhex may provide UV energy absorption for **BUC-68** [92]. No broad and strong emission band presented in the spectrum of the H_6clhex ligand suggested that the absorbed energy is effectively transferred to the Tb(III) center. Comparing to H_6clhex, the bands in the absorption spectrum of **BUC-68** are slightly blue-shifted, along with a new band centered ca. 230 nm occurred. The slight blue shift in the range of 230–300 nm can be attributed to the deprotonation of H_6clhex and the corresponding coordination interactions with Tb, which further confirmed the energy transfer and the "antenna effect" between the H_6clhex ligand and the Tb centers.

3.4. Sensing of small molecules

Recently, small organic molecules like nitroaromatics, organic amines, acetone, acetonitrile and so on, have attracted increasing attention for their environmental biological hazards and threats to human health [93–95]. MOFs-based luminescent switch "on–off" effect is particularly interesting [96]. The potential "on–off" detect of **BUC-68** toward small organic molecules has been investigated, in which 3.0 mg **BUC-68** powder was dispersed into 3.0 mL of isopropanol, ethanol, methanol, acetonitrile, tetrahydrofuran (THF), trichloromethane (THMS), acetone, benzene, propenamide, N,N-Dimethylformamide (DMF), respectively. After 10 min's contact, the luminescence spectra were recorded under excitation wavelength of 230 nm at room temperature. As shown in Fig. 5(a), it is obviously that the luminescence intensity of **BUC-68** was absolutely quenched when it was dispersed in benzene, DMF, and acetone, while the rest of the selected organic solvents have relatively weak effects on the luminescence intensity of **BUC-68**.

Moreover, the quenching effect of acetone has been further studied for the suspensions of **BUC-68**. In detail, **BUC-68** were dispersed in ethanol as the standard suspension, and the content of acetone was gradually enhanced to monitor the luminescence intensity response. As shown in Fig. S5, the luminescent performance of **BUC-68** with various concentrations of acetone from 0 to 50 vol % was measured. For the ethanol suspension of **BUC-68**, an apparent decrease in the luminescence intensity was observed with on-going addition of acetone. The luminescence almost disappeared as the acetone content increased to 50 vol%, indicating that efficient luminescent quenching of **BUC-68** was controlled by acetone. Notably, the limit detection of acetone is determined as 1vol % for **BUC-68**, which is better than the previous studies [93].

In order to understand the luminescent quenching mechanism of **BUC-68** towards these small organic molecules, their UV–Vis absorption spectra and the PXRD of the samples powder that after dispersing in acetone, DMF and benzene were performed. As shown in Fig. 5(b), a strong UV absorption bands ranging from 220 nm to 320 nm for acetone, DMF and benzene were overlapped with the excitation spectra of **BUC-68** (E_m = 545 nm), indicating the presence of an efficient radiative energy transfer process between **BUC-68** and these small molecules [49]. In the process of energy transfer, these small organic solvent molecules like benzene, DMF, and acetone competed with **BUC-68** to absorb UV excitation energy. During the contact with acetone, just a small amount of energy can be available for **BUC-68**, which results its apparent emission spectra decreased. **BUC-68** was stable in benzene, DMF, and acetone solution, which can be affirmed by the PXRD results (Fig. S1). The PXRD results further confirmed the luminescence quenching mechanism of **BUC-68** is not the destruction of its structure, as the PXRD patterns of the pristine and treated **BUC-68**.

Considering its excellent quenching effect on these organic molecules, the detection performance of **BUC-68** toward some selected PPCPs was studied. Ten typical PPCPs like naproxen (NPX), promethazine hydrochloride (PM-HCl), ketoprofen (KP), aspirin (ASA), sulfisoxazole (SF), chloramphenicol (CHL), acrylamide (AM), sulfacetamide (SF), 2-ethylimidazole (2-EI), bisphenol A (BPA) were selected to investigated. Considering the minor effect on the luminescence intensity on **BUC-68**, ethanol (EtOH) was adopted as solvent to dissolved the selected PPCPs. In detail, 3.0 mg **BUC-68** powder was dispersed into 3.0 mL of PPCPs (10^{-4} M, EtOH) solution respectively. After 10 min's contact, the luminescence spectra were recorded under excitation wavelength of 230 nm at room temperature. As shown in Fig. 6(a), the luminescent intensities of **BUC-68** strongly depend on the solvents. Especially, NPX displayed the most serious quenching effect. The rest of the PPCPs have relatively weak effects on the luminescent intensities of **BUC-68**.

Moreover, the quenching effect resulted from NPX was further studied for the suspensions of **BUC-68**. In the experiment, the suspensions of **BUC-68** were achieved by soaking the powder samples

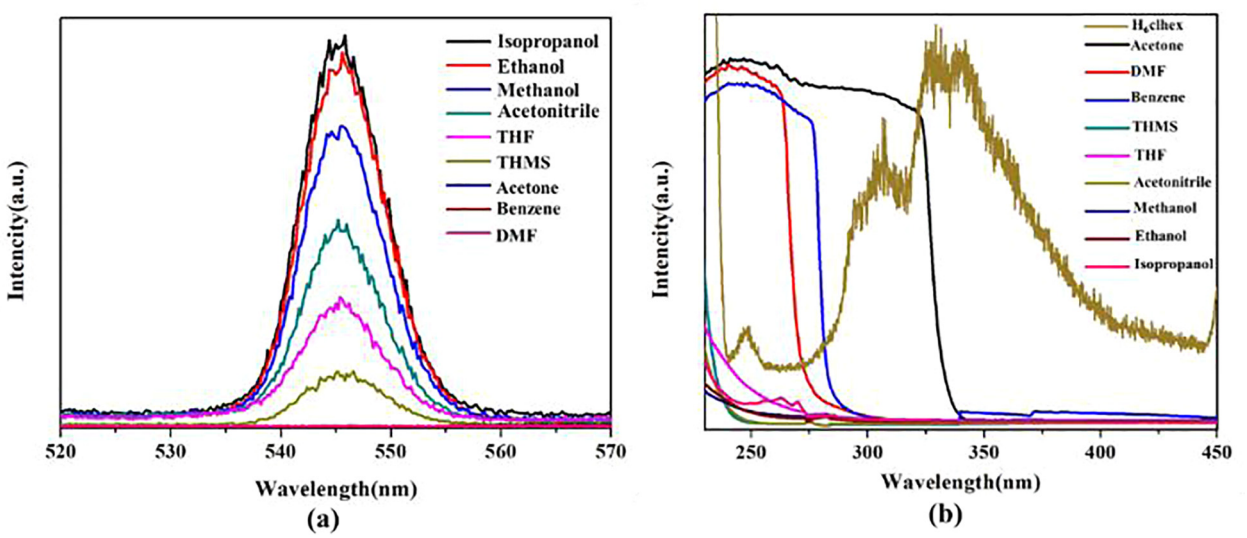

Fig. 5. (a) Emission spectra and intensities for **BUC-68** in different organic solvents; (b) The excitation spectra of **BUC-68** and absorption spectra of various organic solvents.

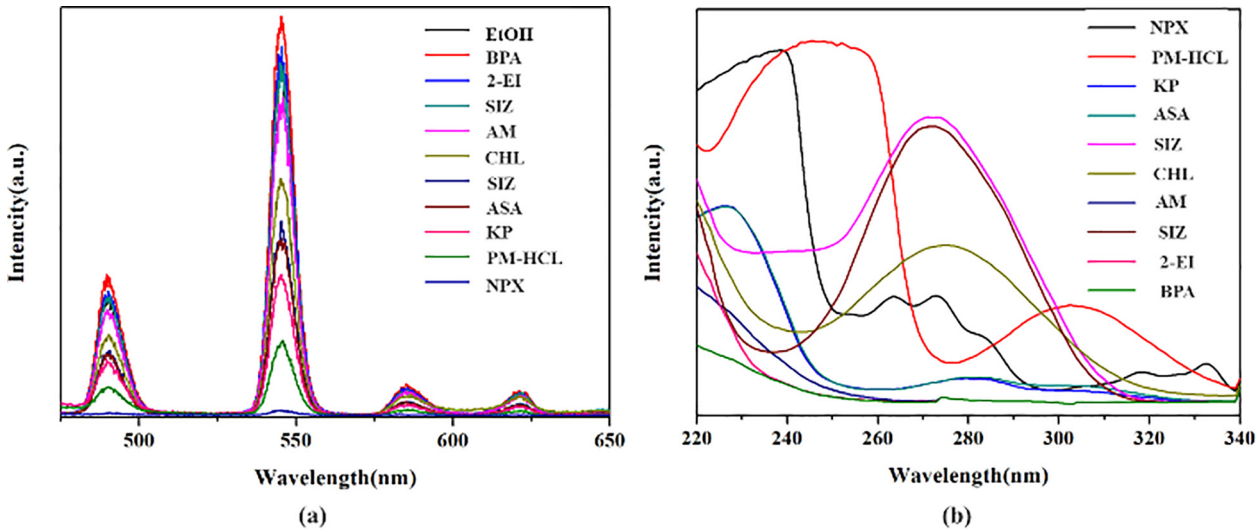

Fig. 6. (a) Emission spectra and intensities for **BUC-68** dispersed in various antibiotics (10^{-4} M, EtOH); (b) The UV–Vis absorption spectra of PPCPs (10^{-4} M) dispersed in EtOH (*Ex* = 230 nm).

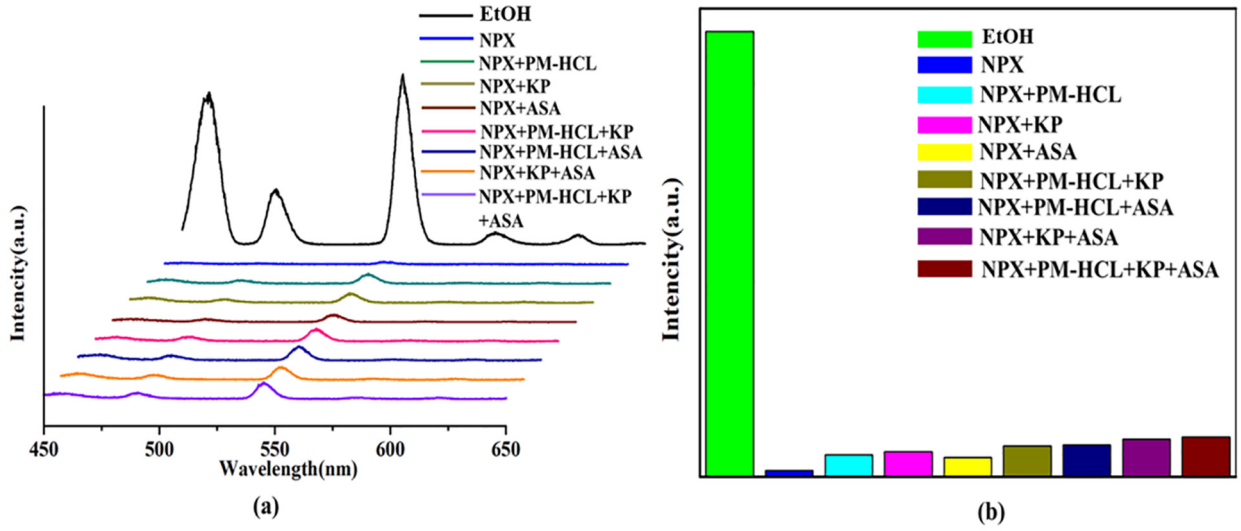

Fig. 7. (a) Emission spectra and intensities for **BUC-68** dispersed in various mixed solution of PPCPs (EtOH); (b) The luminescence intensities for **BUC-68** at 545 nm (*Ex* = 230 nm).

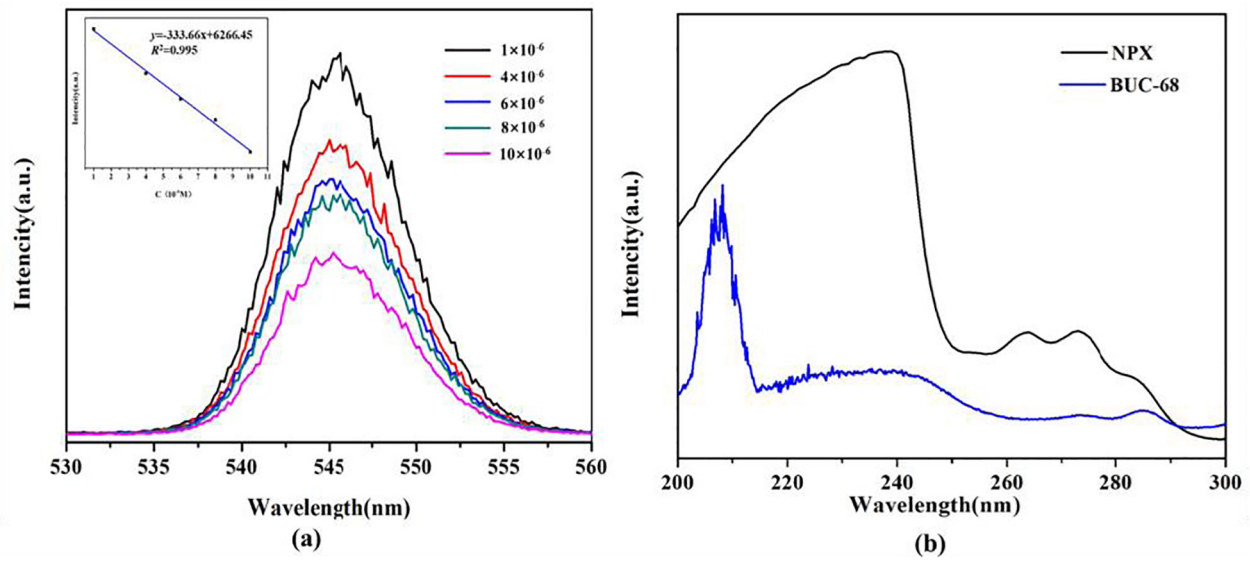

Fig. 8. (a) Emission spectra and intensities for **BUC-68** dispersed in a series of concentration solution of NPX (EtOH) (inset: the inset shows the luminescence intensities for **BUC-68** at 545 nm (*Ex* = 230 nm), (b) The excitation spectra of **BUC-68** and UV–Vis absorption spectra of NPX.

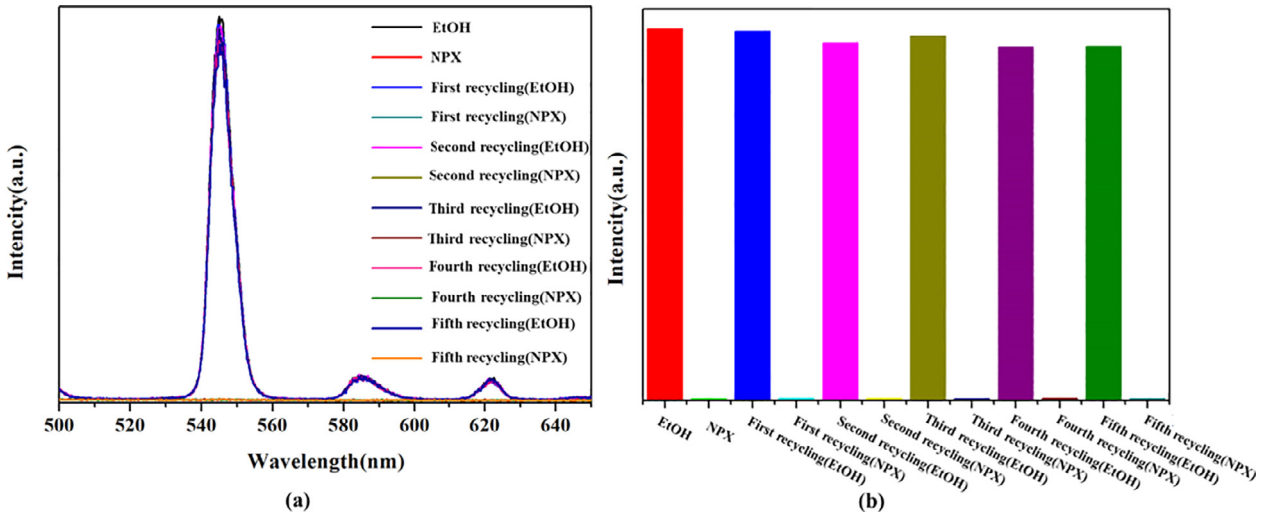

Fig. 9. (a) Luminescence spectra changes during sensing and recycling of **BUC-68**; (b) Luminescence intensity changes during sensing and recycling of **BUC-68** (*Em* = 545 nm).

of **BUC-68** (3 mg) into equal amounts of mixed PPCPs solvents (3 mL), respectively. The results are shown in Fig. 7, it's clear that **BUC-68** can be used as a highly selective sensor for NPX over other PPCPs. The luminescence responses of **BUC-68** were measured in the presence of the different concentrations of NPX. As shown in Fig. 8, when the NPX concentration increased from 10^{-6} M to 10^{-5} M, the luminescence intensity of **BUC-68** was gradually drop off, along with a good linear relationship (correlation coefficient $R^2 = 0.995$) between the emission intensity of **BUC-68** at 545 nm and the concentration of NPX was observed.

The luminescent quenching mechanism of **BUC-68** towards NPX was further investigated by the UV–Vis absorption spectra and excitation spectra. As shown in Fig. 8(b), a strong UV absorption bands ranging from 200 nm to 300 nm for NPX were overlapped with the excitation spectra of **BUC-68** (*Em* = 621 nm), indicating the presence of an efficient radiative energy transfer process between **BUC-68** and NPX [49].

In order to further explore the recyclability and reusability of **BUC-68**, the recycling experiments were performed. As shown in Fig. 9, **BUC-68** exhibited the same degree of luminescence quenching after each cycle, and the recycled samples of **BUC-68** can display the identical fluorescence intensity when being dispersed in ethanol. The PXRD confirmed that the crystallinity of

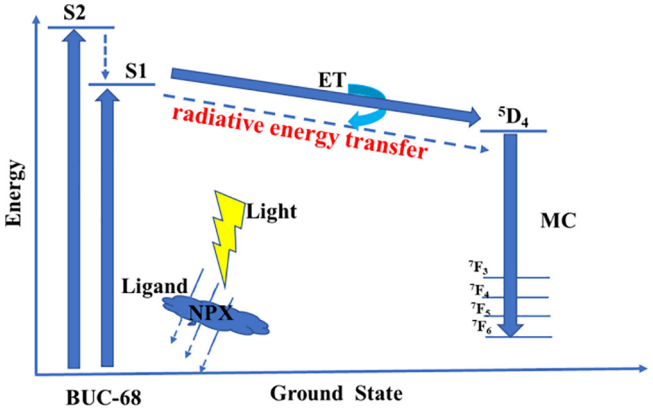

Fig. 10. Luminescence quenching mechanism of **BUC-68** toward NPX.

BUC-68 is still well maintained after multiple use (Fig. S6). The recycling results implied that **BUC-68** has an amazing potential as a long-term luminescent probe for NPX.

The UV–Vis absorption spectra of these PPCPs were shown in Fig. 6(b), which showed that their absorbance at 230 nm varied considerably, while UV–Vis absorption intensity is consistent with the trend of quenching effect to **BUC-68**. The UV–Vis contrast experiment results further confirmed that, the luminescent quenching behaviors were attributed to radiative energy transfer. The schematic diagram of radiative energy transfer process and the proposed mechanism corresponding to the luminescent detect of NPX over **BUC-68** was demonstrated in Fig. 10.

4. Conclusion

In all, a mixed valence Tb (III/IV) MOF(**BUC-68**) based on H_6-clhex ligand have been synthesized under hydrothermal synthesis conditions. **BUC-68** can exhibit very strong luminescence intensity under ultraviolet light through "antenna effect" at room temperature. The luminescent sensing studies demonstrate that **BUC-68** are capable of highly selective detection of small organic molecules and PPCPs through luminescent quenching. The excellent "on–off" switch-functions performance on acetone is attributed to the efficient radiative energy transfer process. **BUC-68** has good performance in selective sensing toward NPX at low detection limit. A further research on making **BUC-68** be a more straightforward sensing probe for NPX and other small molecules is underway.

Acknowledgements

This work was supported by Great Wall Scholars Training Program Project of Beijing Municipality Universities (CIT&TCD20180323), Project of Construction of Innovation Teams and Teacher Career Development for Universities and Colleges Under Beijing Municipality (IDHT20170508), Beijing Talent Project (2018A35), the Fundamental Research Funds for Beijing Universities (X18075/X18076/X18124/X18125/X18276) and Scientific Research Foundation of Beijing University of Civil Engineering and Architecture (KYJJ2017033/KYJJ2017008).

Appendix A. Supplementary data

Supplementary data to this article can be found online at https://doi.org/10.1016/j.poly.2018.11.064.

References

[1] C.C. Wang, Y.S. Ho, Research trend of metal–organic frameworks: a bibliometric analysis, Scientometrics 109 (2016) 1.
[2] O.K. Farha, A.Ö. Yazaydın, I. Eryazici, C.D. Malliakas, B.G. Hauser, M.G. Kanatzidis, S.T. Nguyen, R.Q. Snurr, J.T. Hupp, De novo synthesis of a metal-organic framework material featuring ultrahigh surface area and gas storage capacities, Nat. Chem. 2 (2010) 944.
[3] M. Li, D. Li, M. O'Keeffe, O.M. Yaghi, Topological analysis of metal-organic frameworks with polytopic linkers and/or multiple building units and the minimal transitivity principle, Chem. Rev. 114 (2014) 1343.
[4] X.-D. Du, W. Zheng, X.-H. Yi, J.-P. Zhao, P. Wang, C.-C. Wang, General strategy for lanthanide coordination polymers constructed from 1,1′-ferrocenedicarboxylic acid under hydrothermal conditions, CrystEngComm 20 (2018) 2608.
[5] H. Fu, Z. Wang, X. Wang, P. Wang, C.-C. Wang, Formation mechanism of rod-like ZIF-L and fast phase transformation from ZIF-L to ZIF-8 with morphology changes controlled by polyvinylpyrrolidone and ethanol, CrystEngComm 20 (2018) 1473.
[6] X.D. Du, C.C. Wang, J.G. Liu, X.D. Zhao, J. Zhong, Y.X. Li, J. Li, P. Wang, Extensive and selective adsorption of ZIF-67 towards organic dyes: performance and mechanism, J. Colloid Interface Sci. 506 (2017) 437.
[7] X.D. Du, C.C. Wang, J. Zhong, J.G. Liu, Y.X. Li, P. Wang, Highly efficient removal of Pb^{2+} by a polyoxomolybdate-based organic-inorganic hybrid material {(4-Hap) 4 [Mo_8O_{26}]}, J. Environ. Chem. Eng. 5 (2017) 1866.
[8] H. Kim, S. Yang, S.R. Rao, S. Narayanan, E.A. Kapustin, H. Furukawa, A.S. Umans, O.M. Yaghi, E.N. Wang, Water harvesting from air with metal-organic frameworks powered by natural sunlight, Science 358 (2017) 430.
[9] M. Addicoat, T. Bennett, K. Chapman, D. Denysenko, M. Dincă, H. Doan, T. Easun, M. Eddaoudi, O. Farha, L. Gagliardi, New directions in gas sorption and separation with MOFs: general discussion, Faraday Discuss. 201 (2017) 175.
[10] J.-J. Li, C.-C. Wang, H.-F. Fu, J.-R. Cui, P. Xu, J. Guo, J.-R. Li, High-performance adsorption and separation of anionic dyes in water using a chemically stable graphene-like metal–organic framework, Dalton Trans. 46 (2017) 10197.
[11] X.-Y. Xu, C. Chu, H. Fu, X.-D. Du, P. Wang, W. Zheng, C.-C. Wang, Light-responsive UiO-66-NH_2/Ag_3PO_4 MOF-nanoparticle composites for the capture and release of sulfamethoxazole, Chem. Eng. J. 350 (2018) 436.
[12] X. Zhao, Y. Wei, H. Zhao, Z. Gao, Y. Zhang, L. Zhi, Y. Wang, H. Huang, Functionalized metal-organic frameworks for effective removal of rocephin in aqueous solutions, J. Colloid Interface Sci. 514 (2018) 234.
[13] Y. Peng, Y. Zhang, H. Huang, C. Zhong, Flexibility induced high-performance MOF-based adsorbent for nitroimidazole antibiotics capture, Chem. Eng. J. 333 (2018) 678.
[14] D. Sheng, L. Zhu, C. Xu, C. Xiao, Y. Wang, Y. Wang, L. Chen, J. Diwu, J. Chen, Z. Chai, Efficient and selective uptake of TcO_4^- by a cationic metal-organic framework material with open Ag^+ sites, Environ. Sci. Technol. 51 (2017) 3471.
[15] K.M. Choi, D. Kim, B. Rungtaweevoranit, C.A. Trickett, J.T.D. Barmanbek, A.S. Alshammari, P. Yang, O.M. Yaghi, Plasmon-enhanced photocatalytic CO_2 conversion within metal-organic frameworks under visible light, J. Am. Chem. Soc. 139 (2016) 356.
[16] F.X. Wang, X.H. Yi, C.C. Wang, J.G. Deng, Photocatalytic Cr(VI) reduction and organic-pollutant degradation in a stable 2D coordination polymer, Chin. J. Catal. 38 (2017) 2141.
[17] D.X. Xu, C.C. Wang, P. Wang, J. Li, X.X. Guo, S.J. Gao, Two novel 2D coordination polymers constructed from 5-aminoisophthalic acid and 4,4′-bipyridyl ligands: syntheses, crystal structure, and photocatalytic performance, J. Mol. Struct. 1135 (2017) 129.
[18] C.C. Wang, X.D. Du, J. Li, X.X. Guo, P. Wang, J. Zhang, Photocatalytic Cr(VI) reduction in metal-organic frameworks: a mini-review, Appl. Catal. B 193 (2016) 198.
[19] H.P. Jing, C.C. Wang, Y.W. Zhang, P. Wang, R. Li, Photocatalytic degradation of methylene blue in ZIF-8, RSC Adv. 4 (2014) 54454.
[20] C.C. Wang, J.R. Li, X.L. Lv, Y.Q. Zhang, G. Guo, Photocatalytic organic pollutants degradation in metal–organic frameworks, Energy Environ. Sci. 7 (2014) 2831.
[21] P. García-Holley, B. Schweitzer, T. Islamoglu, Y. Liu, L. Lin, S. Rodriguez, M.H. Weston, J.T. Hupp, D.A. Gómez-Gualdrón, T. Yildirim, Benchmark study of hydrogen storage in metal-organic frameworks under temperature and pressure swing conditions, ACS Energy Lett. 3 (2018) 748.
[22] M.H. Alkordi, Y. Belmabkhout, A. Cairns, M. Eddaoudi, Metal–organic frameworks for H_2 and CH_4 storage: insights on the pore geometry–sorption energetics relationship, Iucrj 4 (2017) 131.
[23] C.X. Chen, Z.W. Wei, J.J. Jiang, S.P. Zheng, H.P. Wang, Q.F. Qiu, C.C. Cao, D. Fenske, C.Y. Su, Dynamic spacer installation for multirole metal-organic frameworks: a new direction toward multifunctional MOFs achieving ultrahigh methane storage working capacity, J. Am. Chem. Soc. 139 (2017) 6034.
[24] F. Gándara, H. Furukawa, S. Lee, O.M. Yaghi, High methane storage capacity in aluminum metal-organic frameworks, J. Am. Chem. Soc. 136 (2014) 5271.
[25] J. Liu, T.Y. Bao, X.Y. Yang, P.P. Zhu, L.H. Wu, J.Q. Sha, L. Zhang, L.Z. Dong, X.L. Cao, Y.Q. Lan, Controllable porosity conversion of metal-organic frameworks composed of natural ingredients for drug delivery, Chem. Commun. 53 (2017) 7804.
[26] H. Zheng, Y. Zhang, L. Liu, W. Wan, P. Guo, A.M. Nyström, X. Zou, One-pot synthesis of metal-organic frameworks with encapsulated target molecules and their applications for controlled drug delivery, J. Am. Chem. Soc. 138 (2015) 962.
[27] W.M. Chen, X.L. Meng, G.L. Zhuang, Z. Wang, M. Kurmoo, Q.Q. Zhao, X.P. Wang, B. Shan, C.H. Tung, D. Sun, A superior fluorescent sensor for Al^{3+} and UO_2^{2+} based on a Co(II) metal–organic framework with exposed pyrimidyl Lewis base sites, J. Mater. Chem. A 5 (2017) 13079.
[28] J.-W. Cui, S.-X. Hou, Y.-H. Li, G.-H. Cui, A multifunctional Ni(II) coordination polymer: synthesis, crystal structure and applications as a luminescent sensor, electrochemical probe, and photocatalyst, Dalton Trans. 46 (2017) 16911.
[29] J. Hao, B. Yu, K.V. Hecke, G. Cui, A series of d10 metal coordination polymers based on a flexible bis(2-methylbenzimidazole) ligand and different carboxylates: synthesis, structures, photoluminescence and catalytic properties, CrystEngComm 17 (2015) 2279.
[30] C. Wang, G. Guo, P. Wang, Two sodium and lanthanide(III) MOFs based on oxalate and V-shaped 4,4′-oxybis(benzoate) ligands: hydrothermal synthesis, crystal structure, and luminescence properties, J. Mol. Struct. 1032 (2013) 93.
[31] Y. Zhu, W.Y. Wang, M.W. Guo, G. Li, H.J. Lu, An unprecedented 1-D mixed-valence Cu(II)/Cu(I) metal-organic framework bearing 2-phenyl imidazole dicarboxylates, Inorg. Chem. Commun. 14 (2011) 1432.
[32] S. Benmansour, A. Abhervé, P. Gómezclaramunt, C. Vallésgarcía, C.J. Gomezgarcia, Nano-sheets of 2D magnetic and conducting Fe(II)/Fe(III) mixed-valence MOFs, ACS Appl. Mater. Interfaces 9 (2017) 26210.
[33] S.R. Miller, D. Heurtaux, T. Baati, P. Horcajada, J.M. Grenèche, C. Serre, Biodegradable therapeutic MOFs for the delivery of bioactive molecules, Chem. Commun. 46 (2010) 4526.
[34] J.W. Yoon, Y.K. Seo, Y.K. Hwang, J.S. Chang, H. Leclerc, S. Wuttke, P. Bazin, A. Vimont, M. Daturi, E. Bloch, Inside cover: controlled reducibility of a metal–

organic framework with coordinatively unsaturated sites for preferential gas sorption (Angew. Chem. Int. Ed. 34/2010), Angew. Chem. Int. Ed. 49 (2010) 5949.
[35] P. Kar, R. Haldar, C.J. Gómezgarcía, A. Ghosh, Antiferromagnetic porous metal-organic framework containing mixed-valence $[Mn^{II}_4Mn^{III}_2(\mu_4\text{-}O)_2]^{10+}$ units with catecholase activity and selective gas adsorption, Inorg. Chem. 51 (2012) 4265.
[36] H. Wang, X. Yuan, Y. Wu, G. Zeng, X. Chen, L. Leng, H. Li, Synthesis and applications of novel graphitic carbon nitride/metal-organic frameworks mesoporous photocatalyst for dyes removal, Appl. Catal. B 174–175 (2015) 445.
[37] F. Gérard, M. Franck, M. Mathieu, S. Christian, D. Marie-Liesse, G. Jean-Marc, T. Jean-Marie, Mixed-valence Li/Fe-based metal-organic frameworks with both reversible redox and sorption properties, Angew. Chem. Int. Ed. 46 (2007) 3259.
[38] J. He, J.X. Zhang, C.K. Tsang, Z. Xu, Y.G. Yin, D. Li, S.W. Ng, Mixed-valence CuIICuI15I17 cluster builds up a 3D metal–organic framework with paramagnetic and thermochromic characteristics, Inorg. Chem. 47 (2008) 7948.
[39] C.H. Hendon, D. Tiana, M. Fontecave, C. Sanchez, L. D'Arras, C. Sassoye, L. Rozes, C. Mellotdraznieks, A. Walsh, Engineering the optical response of the titanium-MIL-125 metal-organic framework through ligand functionalization, J. Am. Chem. Soc. 135 (2013) 10942.
[40] H. ŌKawa, M. Sadakiyo, T. Yamada, M. Maesato, M. Ohba, H. Kitagawa, Proton-conductive magnetic metal–organic frameworks, {NR3(CH2COOH)}[MaIIMbIII(ox)3]: effect of carboxyl residue upon proton conduction, J. Am. Chem. Soc. 135 (2016) 2256.
[41] B. Cai, Y. Ren, H. Jiang, D. Zheng, D. Shi, Y. Qian, J. Chen, A mixed-valence lanthanide metal–organic framework, templated by 2,2′-bipyridine formed reaction: synthesis, structure, and luminescent properties, CrystEngComm 14 (2012) 5285.
[42] K. Müller-Buschbaum, Y. Mokaddem, MOFs by solvent free high temperature synthesis exemplified by ∞ 3 $[Eu_3(Tz*)6(Tz*H)_2]$, Solid State Sci. 10 (2008) 416.
[43] W. Liu, L. Liu, Y. Wang, L. Chen, J.A. Mcleod, L. Yang, J. Zhao, Z. Liu, J. Diwu, Z. Chai, Tuning Mixed-Valent Eu^{2+}/Eu^{3+} in Strontium Formate Frameworks for Multichannel Photoluminescence, Chemistry (Weinheim an der Bergstrasse, Germany) 22 (2016) 11170.
[44] L.E. Kreno, K. Leong, O.K. Farha, M. Allendorf, R.P.V. Duyne, J.T. Hupp, Metal-organic framework materials as chemical sensors, Chem. Rev. 112 (2012) 1105.
[45] J.N. Hao, B. Yan, A water-stable lanthanide-functionalized MOF as a highly selective and sensitive fluorescent probe for Cd(2.), Chem. Commun. 51 (2015) 7737.
[46] H.L. Jiang, Y. Tatsu, Z.H. Lu, Q. Xu, Non-, micro-, and mesoporous metal-organic framework isomers: reversible transformation, fluorescence sensing, and large molecule separation, J. Am. Chem. Soc. 132 (2010) 5586.
[47] Z. Chen, Y. Sun, L. Zhang, D. Sun, F. Liu, Q. Meng, R. Wang, D. Sun, A tubular europium-organic framework exhibiting selective sensing of Fe^{3+} and Al^{3+} over mixed metal ions, Chem. Commun. 49 (2013) 11557.
[48] X.Y. Ren, L.H. Lu, Luminescent nanoscale metal–organic frameworks for chemical sensing, Chin. Chem. Lett. 26 (2015) 1439.
[49] W.P. Lustig, S. Mukherjee, N.D. Rudd, A.V. Desai, J. Li, S.K. Ghosh, Metal-organic frameworks: functional luminescent and photonic materials for sensing applications, Chem. Soc. Rev. 46 (2017) 3242.
[50] J.J. Li, C.C. Wang, H.F. Fu, J.R. Cui, P. Xu, J. Guo, J.R. Li, High-performance adsorption and separation of anionic dyes in water using a chemically stable graphene-like metal-organic framework, Dalton Trans. 46 (2017) 10197.
[51] X. Li, D.Y. Wei, S.J. Huang, Y.Q. Zheng, Syntheses and characterization of novel lanthanide adamantine–dicarboxylate coordination complexes, J. Solid State Chem. 182 (2009) 95.
[52] J.J. Li, C.C. Wang, J. Guo, J.R. Cui, P. Wang, Two zigzag chain-like lanthanide(III) coordination polymers based on the rigid 1,3-adamantanedicarboxylic acid ligand: crystal structure, luminescence and magnetic properties, Polyhedron 126 (2017) 17.
[53] P. Thuéry, B. Masci, Two- and three-dimensional europium–organic assemblies with the all-cis and all-trans isomers of 1,2,3,4,5,6-cyclohexanehexacarboxylic acid, Cryst. Des. 10 (2010) 3626.
[54] P. Thuéry, A lanthanide ion-decorated uranyl–organic two-dimensional assembly with all-cis 1,2,3,4,5,6-cyclohexanehexacarboxylic acid, Cryst. Growth Des. 10 (2010) 2061.
[55] G. Lu, Syntheses and crystal structures of four lanthanide complexes based on two tri-protonated hexacarboxylic acids of 1,2,3,4,5,6-cyclohexane-hexacarboxylic acid and mellitic acid, J. Coord. Chem. 68 (2015) 1800.
[56] L. Cañadillas-Delgado, O. Fabelo, J. Pasán, M. Julve, F. Lloret, C. Ruiz-Pérez, All-cis-1,2,3,4,5,6-cyclohexanehexacarboxylate two-dimensional gadolinium(III) complexes: synthesis, X-ray crystal structure and magnetic properties, Polyhedron 29 (2010) 188.
[57] W. Jing, Z.Q. Liu, S.U. Ting-Ting, Synthesis, structure and luminescent property of a zinc(II) coordination polymer incorporating flexible cyclohexane-1,2,3,4,5,6-hexacarboxylate ligand, Chem. Res. Chin. Univ. 27 (2011) 354.
[58] H. Xie, G. Lu, Syntheses and crystal structures of four lanthanide complexes based on two tri-protonated hexacarboxylic acids of 1,2,3,4,5,6-cyclohexane-hexacarboxylic acid and mellitic acid, J. Coord. Chem. 68 (2015) 1800.
[59] N. Sabbatini, M. Guardigli, J.M. Lehn, Luminescent lanthanide complexes as photochemical supramolecular devices, Coord. Chem. Rev. 123 (1993) 201.
[60] Bruker AXS, SMART, Version 5.611, Bruker AXS, Madison, WI, USA, 2000.
[61] Bruker AXS, SAINT, Version 6.28, Bruker AXS, Madison, WI, USA, 2003.
[62] SADABS, V2.03, Bruker AXS, Madison, WI, 2000.
[63] G.M. Sheldrick, Acta Crystallogr. A 71 (2015) 3.
[64] J. Wang, Y.H. Zhang, M.L. Tong, Two new 3D metal-organic frameworks of nanoscale cages constructed by Cd(II) and conformationally-flexible cyclohexanehexacarboxylate, Chem. Commun. 30 (2006) 3166.
[65] W. Liu, G. Zhao, M. An, L. Chang, Solvothermal synthesis of nanostructured $BiVO_4$ with highly exposed (0 1 0) facets and enhanced sunlight-driven photocatalytic properties, Appl. Surf. Sci. 357 (2015) 1053.
[66] J. Zhang, C.C. Wang, P. Wang, X.X. Guo, S.J. Gao, Silver-based coordination complexes of carboxylate ligands: crystal structures, luminescence and photocatalytic properties, Transition Met. Chem. 41 (2016) 1.
[67] X.H. Yi, F.X. Wang, X.D. Du, H. Fu, C.C. Wang, Highly efficient photocatalytic Cr (VI) reduction and organic pollutants degradation of two new bifunctional 2D Cd/Co-based MOFs, Polyhedron 1327 (2018).
[68] E.R. Souza, I.G.N. Silva, E.E.S. Teotonio, M.C.F.C. Felinto, H.F. Brito, Optical properties of red, green and blue emitting rare earth benzenetricarboxylate compounds, J. Lumin. 130 (2010) 283.
[69] W.A.N.G. Jing, X.U. Min, S.U. Ting-Ting, Hydrothermal synthesis and crystal structure of a novel lanthanide coordination polymer bridged by flexible cyclohexane-1,2,3,4,5,6-hexacarboxylate and rigid oxalate ligands, Chin. J. Inorg. Chem. 27 (2011) 737.
[70] M. Farina, M. Grassi, G.D. Silvestro, Stereochemical study of 1,2,3,4,5,6-(hexamethoxycarbonyl)cyclohexanes, Cheminform 107 (1985) 5100.
[71] W. Bi, R. Cao, D. Sun, D. Yuan, X. Li, Y. Wang, X. Li, M. Hong, Isomer separation, conformation control of flexible cyclohexanedicarboxylate ligand in cadmium complexes, Chem. Commun. 10 (2004) 2104.
[72] N. Otto, T. Opatz, Heterocycles from α-Aminonitriles, Chem.-A Eur. J. 20 (2014) 13064.
[73] J. Wang, Z.J. Lin, Y.C. Ou, Y. Shen, R. Herchel, M.L. Tong, Coordination chemistry of conformation-flexible 1,2,3,4,5,6-cyclohexanehexacarboxylate: trapping various conformations in metal-organic frameworks, Chem.-A Eur. J. 14 (2008) 7218.
[74] J. Wang, L.L. Zheng, C.J. Li, A. Yanzhen Zheng, M.L. Tong, Coexistence of planar and chair-shaped cyclic water hexamers in a unique cyclohexanehexacarboxylate-bridged metal–organic framework, Cryst. Growth Des. 6 (2006) 357.
[75] H.Y. Li, Y.L. Wei, X.Y. Dong, S.Q. Zang, T.C.W. Mak, Novel Tb-MOF embedded with viologen species for multi-photofunctionality: photochromism, photomodulated fluorescence, and luminescent pH sensing, Chem. Mater. 27 (2015) 1327.
[76] S.E. Russell, C. Gosset, X. Agache, C. Volkringer, N. Henry, R. Decadt, R.V. Deun, M. Visseaux, T. Loiseau, A new series of trivalent lanthanide (Ce, Pr, Nd, Sm, Eu, Gd, Tb, Dy) coordination polymers with a 1,2-cyclohexanedicarboxylate ligand: synthesis, crystal structure, luminescence and catalytic properties, CrystEngComm 18 (2016) 3594.
[77] V. Kumar, S. Som, V. Kumar, V. Kumar, O.M. Ntwaeaborwa, E. Coetsee, H.C. Swart, Tunable and white emission from $ZnO:Tb^{3+}$ nanophosphors for solid state lighting applications, Chem. Eng. J. 255 (2014) 541.
[78] K.G. Tshabalala, I.M. Nagpure, H.C. Swart, O.M. Ntwaeaborwa, S.H. Cho, J.K. Park, Enhanced green emission from UV down-converting Ce^{3+}–Tb^{3+} co-activated $ZnAl_2O_4$ phosphor, J. Vacuum Sci. Technol. B 30 (2012) 31401.
[79] T. Matsuzawa, Y. Aoki, N. Takeuchi, Y. Murayama, ChemInform abstract: a new long phosphorescent phosphor with high brightness, SrAl2O4:Eu^{2+}, Dy^{3+}, Cheminform 27 (2010) no.
[80] T. Matsuzawa, Y. Aoki, N. Takeuchi, Y. Murayama, A new long phosphorescent phosphor with high brightness, SrAl2O4:Eu^{2+}, Dy^{3+}, Cheminform 27 (2010).
[81] R.K. Verma, K. Kumar, S.B. Rai, Inter-conversion of Tb3+ and Tb4+ states and its fluorescence properties in MO–Al2O3: Tb (M=Mg, Ca, Sr, Ba) phosphor materials, Solid State Sci. 12 (2010) 1146.
[82] G. Blasse, G.J. Dirksen, A. Meyerink, D.R. Terrell, L. Neyens, An efficient green-emitting luminescent material: Tb^{3+}-activated monoclinic Gd_2O_3, Mater. Chem. Phys. 19 (1988) 547.
[83] G. Blasse, Luminescence of inorganic solids: from isolated centres to concentrated systems, Prog. Solid State Chem. 18 (1988) 79.
[84] P. Dorenbos, Predictability of 5d level positions of the triply ionized lanthanides in halogenides and chalcogenides, J. Lumin. 87–89 (2000) 970.
[85] A.M. Srivastava, Luminescence of Eu^{3+}, Tb^{3+} and Bi^{3+} in the Weberite $NaGdSb_2O_7$, J. Lumin. 69 (1996) 301.
[86] B. Liu, W.P. Wu, L. Hou, Y.Y. Wang, Four uncommon nanocage-based Ln-MOFs: highly selective luminescent sensing for Cu^{2+} ions and selective CO_2 capture, Chem. Commun. 50 (2014) 8731.
[87] N. Campagnol, E.R. Souza, D.E. De Vos, K. Binnemans, J. Fransaer, Luminescent terbium-containing metal-organic framework films: new approaches for the electrochemical synthesis and application as detectors for explosives, Chem. Commun. 50 (2014) 12545.
[88] T.M. Reineke, M. Eddaoudi, Michael Fehr, A. Douglas Kelley, O.M. Yaghi, From condensed lanthanide coordination solids to microporous frameworks having accessible metal sites, J. Am. Chem. Soc. 121 (1999) 1651.
[89] S. Zhang, Y. Yang, Z.Q. Xia, X.Y. Liu, Q. Yang, Q. Wei, G. Xie, S.P. Chen, S.L. Gao, Eu-MOFs with 2-(4-carboxyphenyl)imidazo[4,5-f]-1,10-phenanthroline and ditopic carboxylates as coligands: synthesis, structure, high thermostability, and luminescence properties, Inorg. Chem. 53 (2014) 10952.
[90] K.A. White, D.A. Chengelis, M. Zeller, S.J. Geib, J. Szakos, S. Petoud, N.L. Rosi, Near-infrared emitting ytterbium metal-organic frameworks with tunable excitation properties, Chem. Commun. 30 (2009) 4506.

[91] J. Zhang, P.D. Badger, S.J. Geib, S. Petoud, Sensitization of near-infrared-emitting lanthanide cations in solution by tropolonate ligands, Angew. Chem., Int. Ed. Engl. 44 (2010) 2508.
[92] L.N. Jia, L. Hou, L. Wei, X.J. Jing, B. Liu, Y.Y. Wang, Q.Z. Shi, Five sra topological Ln(III)-MOFs based on novel metal-carboxylate/cl chain: structure, near-infrared luminescence and magnetic properties, Cryst. Growth Des. 13 (2013) 1570.
[93] S.S. Zhao, J. Yang, Y.Y. Liu, J.F. Ma, Fluorescent aromatic tag-functionalized MOFs for highly selective sensing of metal ions and small organic molecules, Inorg. Chem. 55 (2016) 2261.
[94] S.S. Nagarkar, B. Joarder, A.K. Chaudhari, S. Mukherjee, S.K. Ghosh, Highly selective detection of nitro explosives by a luminescent metal-organic framework, Angew. Chem. Int. Ed. 52 (2013) 2881.
[95] H. Fu, X. Wang, P. Wang, Z. Wang, H. Ren, C.C. Wang, Enhanced acetone sensing performance of Au nanoparticle modified porous tube-like ZnO derived from rod-like ZIF-L, Dalton Trans. 9014 (2018).
[96] J.E. Kwon, S. Lee, Y. You, K.H. Baek, K. Ohkubo, J. Cho, S. Fukuzumi, I. Shin, S.Y. Park, W. Nam, Fluorescent zinc sensor with minimized proton-induced interferences: photophysical mechanism for fluorescence turn-on response and detection of endogenous free zinc ions, Inorg. Chem. 51 (2012) 8760.